PLASTIC DEFORMATION OF ALUMINIUM-BICRYSTALS

Max-Planck Project Report

J.-C. Kuo, S. Zaefferer, D. Raabe

Max-Planck-Institut für Eisenforschung
Max-Planck-Str. 1
40237 Düsseldorf
Germany

January 2004, Max-Planck-Society
*http://*www.mpg.de *http://*www.mpie.de *http://edoc.mpg.de/*

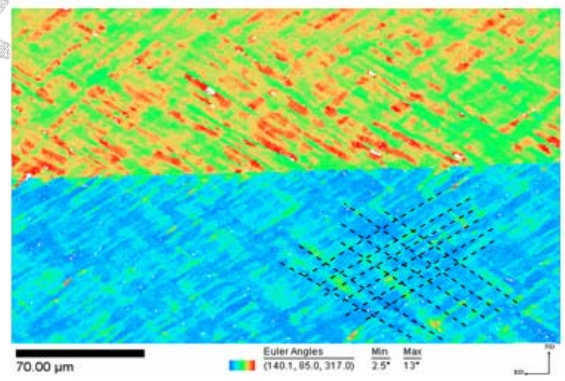

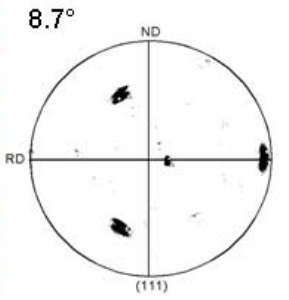

Report abstract

This progress report discusses the deformation behaviour of an aluminium-bicrystal with a symmetrical <112> tilt boundary and an initial misorientation of 8.7°. The specimen was compressed in a channel die to 30% engineering thickness reduction at room temperature. Afterwards the crystal orientations were determined by electron backscatter diffraction (EBSD) and the plastic strain distribution was measured by photogrametry. It was found that the two abutting crystals close to the grain boundary rotate towards each other, whereas the grain interiors increase their mutual misorientation during plastic loading.

1 Introduction

Grain boundaries represent natural obstacles to the motion of dislocations during plastic straining of crystalline matter. As such they may be the cause of grain-scale heterogeneity in terms of the mismatch of the elastic-plastic strain rate, internal stress, and crystallographic reorientation rate fields. Investigating such nonhomogeneity systematically as a function of the grain boundary character under well defined mechanical boundary conditions is important for better understanding grain scale and grain boundary micromechanics as well as micro- and nanoscale texture evolution.

A hierarchical approach to study grain-scale plastic heterogeneity consists in investigating the influence of isolated *grain boundaries* (bicrystals) [1-5], *triple junctions* (tri-crystals) [6,7] and simple *grain boundary networks* (oligocrystals) [8-11] under well defined external loading conditions.

Prior investigations of bicrystal deformation by Livingston and Chalmers [1] have shown that at least four slip systems are required for explaining the observed macroscopic plastic incompatibility at the boundary. The additional operation of second slip systems due to the elastic incompatibility at the grain boundary was suggested by Hook and Hirth [3-4]. Both previous studies were focused on intergranular incompatibilities, that is, on plastic and elastic incompatibility across the grain boundary. Rey and Zaoui [2,5,8] have shown that the internal stress due to intragranular incompatibilities at the grain boundary results in additional slip systems as well as a pronounced hardening.

Most of these previous studies essentially addressed the question of elastic-plastic incompatibility at grain boundaries on a mesoscopic scale. In the present work we take a somewhat different approach in that we jointly investigate the spatial distribution of the plastic strain and the texture evolution at grain boundaries on different scales, ranging from nanoscale texture determination to micro- and macroscopic measurements of the overall strain distribution within the sample surface. This scale-bridging experimental approach helps us to

get a better survey on the influence of the heterogeneous conditions imposed by the respective contact and loading situations and their influence on the local microstructure.

2 Experimental Methods

2.1 Sample preparation and deformation setup

An aluminium-bicrystal with a symmetrical <112> tilt boundary with an initial misorientation of 8.7° was grown by a modified Bridgeman technique. Figure 1 shows the (111) pole figure of the initial specimen prior to mechanical loading. A schematic drawing of the channel die setup is shown in Figure 2. The sample is loaded along the compression direction (ND) and it extends in the elongation direction (RD). The front sides of the channel prevent displacements along the transverse direction (TD). During deformation the normal of the grain boundary was parallel to the compression direction (ND), as shown in Figure 2a. The sample size amounted to 17×20 mm^2 in cross section and 4 mm in sample thickness. Plane strain compression experiments were carried out at a strain rate of 1.7×10^{-5} s^{-1} in a channel die set-up, as shown in Figure 2b. In order to reduce frictional effects and to protect the grey scale pattern on the specimen surface as required for the photogrametry analysis between the subsequent straining steps the specimen was wrapped in a Teflon foil with 80 μm thickness.

2.2 Sample characterization

Before deformation the ND-RD (ND: compression direction, RD: elongation direction) sample surface was mechanically polished and the initial orientations were determined using automatic crystal orientation mapping (ACOM) by automatic analysis of electron backscatter diffraction (EBSD) patterns in a scanning electron microscope (SEM). Subsequently a fine white colour spray was applied onto the polished surface in order to suppress metallic reflections. After that fine dots of black colour were sprayed on the white background. This pattern gave excellent contrast for pattern recognition. Plane strain compression was performed in steps of about 5% engineering plastic reduction up to a total thickness reduction

of 30%. After each deformation step including the initial undeformed state, the colour patterns on the sample surface were registered as digital images by use of a high resolution CCD-camera. After 30% deformation the deformed sample surface was once again mechanically polished and a final orientation mapping was measured by ACOM mapping the entire surface using a lateral step size of 100 μm. In addition high resolution orientation maps were measured close to the grain boundary as well as in the interiors of the abutting crystals using a step size of 70 nm on areas 300 μm×100 μm.

The plastic strain was determined by use of photogrametry. The central point of this technique is a matching procedure between an image (pattern) of the undeformed state and that of the deformed state which is quantified in terms of a correlation coefficient C. The distribution of grey scale values of a facet (rectangular area) in the pattern taken from the undeformed state corresponds to that of the same area in the deformed state, if the correlation coefficient C assumes a minimum. C is defined as

$$C = 1 - \int_{\Delta S} f_s(x_s, y_s)\, f_d(x_d, y_d)\, dxdy \Big/ \sqrt{\int_{\Delta S} f_s(x_s, y_s)^2\, dxdy \int_{\Delta S} f_d(x_d, y_d)^2\, dxdy} \qquad (1)$$

where ΔS is the inspected area of the correlation pattern in the initial image, and $f_s(x_s, y_s)$ and $f_d(x_d, y_d)$ are the grey level values in the reference and deformed regions, respectively [9,10,12]. After the matching procedure, the displacement field on the surface, and from this the in-plane strain distribution can be derived from the corresponding coordinates in the initial and deformed states. The in-plane plastic strain mapping can be categorized into two different types, an accumulated and an incremental strain mapping. The former is obtained by comparing the image after each deformation step with respect to the initial image. The latter is determined by comparing the images taken before and after each deformation step.

3 Results and discussion

3.1 Plastic strain mapping

From the strain components the plastic von Mises strain distribution was calculated. After 5% thickness reduction the distribution of the plastic von Mises strain was quite homogeneous, Figure 3a. After 30% engineering thickness reduction both crystals revealed macroscopic deformation bands, which do not correspond to crystallographic slip directions, Figure 3b. Although the initial orientations of both crystals were symmetric with respect to the grain boundary plane and with respect to the compression direction, the strain distribution in both crystals was very different. While the upper crystal showed high accumulated stresses, the lower one was much less deformed. The above results suggest that the channel die experiment promotes heterogeneous deformation patterns, which are to a large extent influenced by the form of the sample and friction between the tool and the sample.

3.2 Orientation mapping

Crystal orientation maps were measured close to the grain boundary and inside the two abutting crystals in areas which had undergone similar accumulated plastic straining. The results are shown in Figure 4 in form of misorientation maps where the colour coding corresponds to the angular deviation of a given point with respect to each initial orientation. All three areas show similar microstructures consisting of two sets of parallel bands of similar orientations. The arrangement of the parallel nanoscaled bands in each of the three mappings establishes a highly lamellar microstructure in which the in-grain orientation systematically fluctuates in the form of forward and backward orientation changes. The resulting overall orientation spread arising from such microtexture patterning can be observed in the form of orientation traces in the {111} pole figures given in Figure 5. A comparison of the texture maps taken from the grain interiors (Figures 4a and 4c) with that taken across the grain boundary (Figure 4b) shows that the distance of these bands is smaller in the vicinity of the grain boundary. Also, compared to the misorientations in the grain interiors the misorientations in the immediate vicinity of the grain boundary are smaller.

Figure 5a and Figure 5b show the different {111} pole figures of areas near the grain boundary and in the interiors of the two crystals which were obtained from the measured EBSD data. The data clearly show that the grain interiors reveal after straining a larger mutual misorientation than the areas close to the interface. Compared to the initial orientations before deformation the areas close to the grain boundary have rotated *towards* each other, while the areas with a distance of 2mm away from the grain boundary have *increased* their misorientation. This is consistent with the observations of the misorientation gradients mentioned above.

4 Conclusions

We have investigated the deformation behaviour of an aluminium-bicrystal with a symmetrical <112> tilt boundary and an initial misorientation of 8.7°. The specimen was compressed in a channel die to 30% engineering thickness reduction at room temperature. We jointly characterized the lateral fields of the crystallographic lattice rotations and plastic strains. The plastic strain distribution was determined by photogrametry. We observed a strong heterogeneity of the strain in the symmetric bicrystal, i.e. an asymmetric strain distribution was found although the crystal orientations and the boundary plane were symmetric with respect to loading. Crystal lattice rotations were determined by means of electron backscatter diffraction in a high-resolution-SEM. It was found that close to the grain boundary the crystals rotated towards each other. In contrast, the grain interiors revealed an increase of their misorientation.

5 References

1 Livingston, J.D., Chalmers, B., *Acta Metall.*, 1957, **5**, 322.
2 Rey, C., Zaoui, A., *Acta Metall.*, 1980, **28**, 687.
3 Hook, R.E., Hirth, J.P., *Acta Metall.*, 1967, **15**, 535.
4 Hook, R.E., Hirth, J.P., *Acta Metall.*, 1967, **15**, 1099.
5 Rey, C., Zaoui, A., *Acta Metall.*, 1982, **30**, 523.
6 Randle, V., Hansen, N. and Juul Jensen, D. *Phil. Mag.*, 1996, **A73**, 265.
7 Davies, R.K. and Randle, V., *Mater. Sc. Eng.*, 2000, **A283**, 251.
8 Rey, C., *Rev. Phy. Appl.*, 1988, **23**, 491.
9 Raabe, D., Sachtleber, M., Zhao, Z., Roters, F., Zaefferer, S., *Acta mater.*, 2001, **49**, 3433.
10 Sachtleber, M., Zhao, Z., Raabe, D., *Mater. Sc. Eng.* , 2002, **A336**, 81.
11 Delaire, F., Raphanel, J.L., and Rey, C., *Acta Mater.*, 2000, **48**, 1075.
12 Vacher, P., Dumoulin, S., Morestin, F. and Mguil-Touchal, S. *Proc. Inst. Mech. Eng. Part C.J. Mech. Eng. Sci.*, 1999, **213**, 811.
13 Zaefferer, S., J.-C. Kuo, Z. Zhao, M. Winning, D. Raabe: Acta Materialia 51 (2003) 4719-4735.

6 Figures

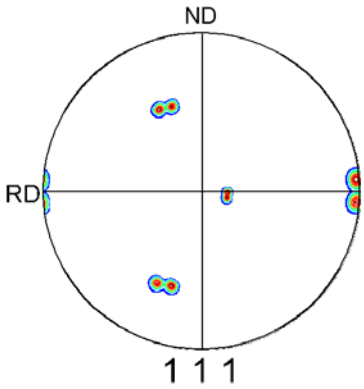

Figure 1: {111} pole figure of the undeformed bicrystal with a symmetrical <112> tilt grain boundary with an initial misorientation of 8.7°.

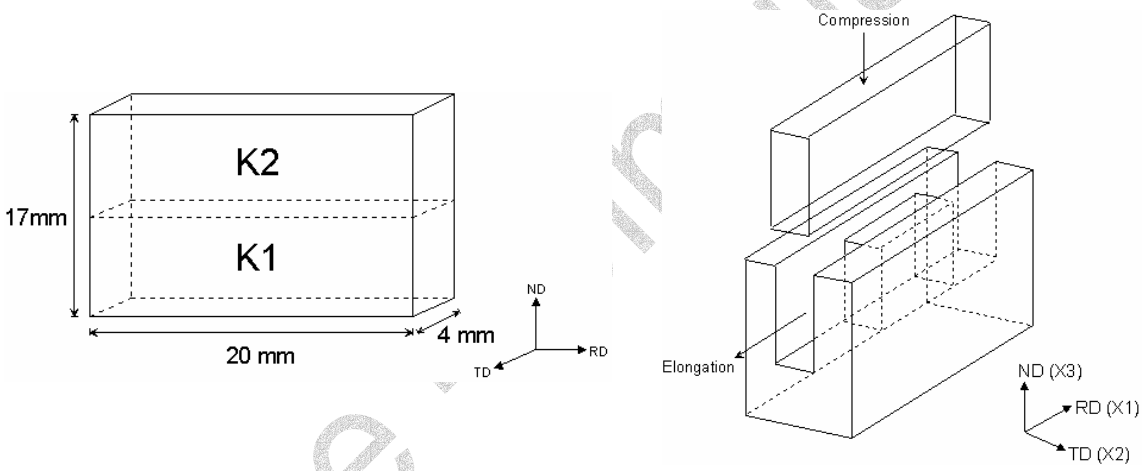

(a) (b)

Figure 2: Schematical drawing of the bicrystal (a) and of the experimental set-up (b).

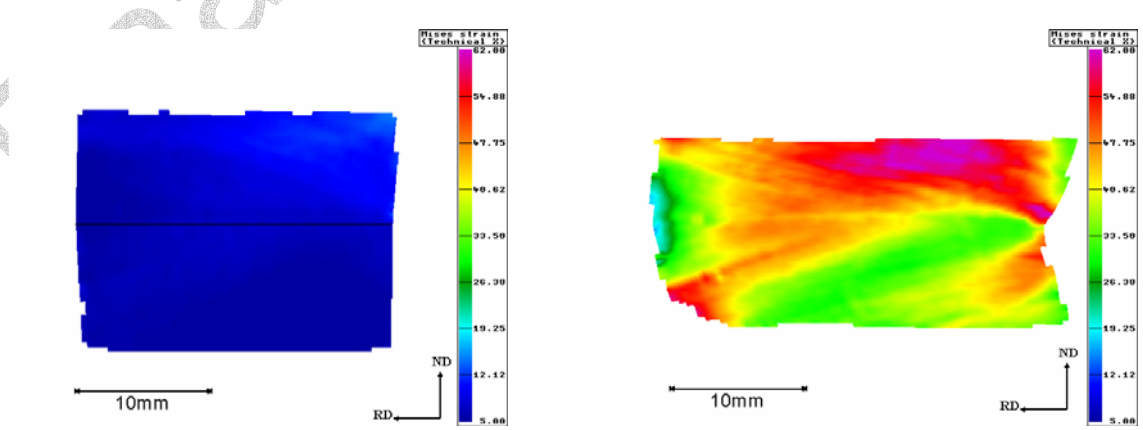

(a) (b)

Figure 3: Spatial distributions of the von Mises strain obtained by measurement (a) after 5% and (b) after 30% deformation.

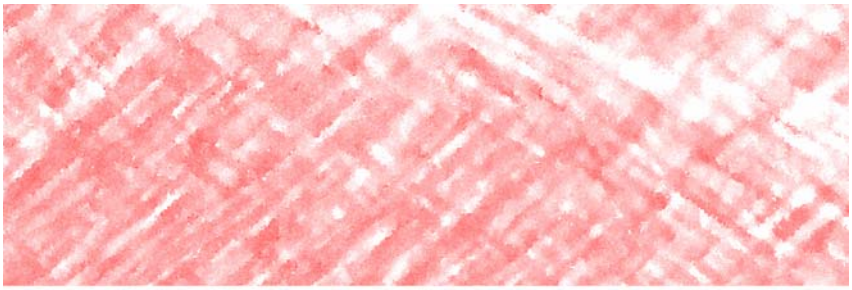

(a) crystal K2, 2mm away from the grain boundary

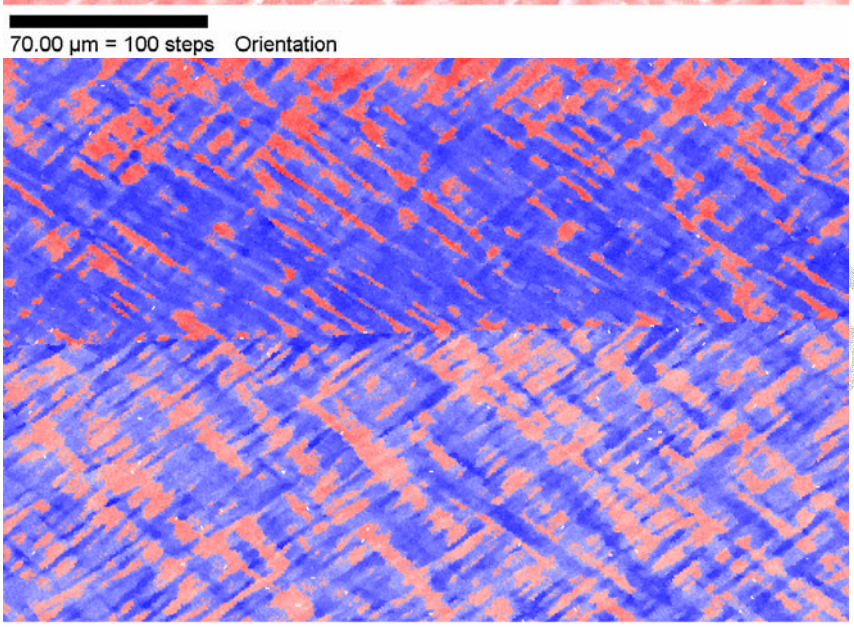

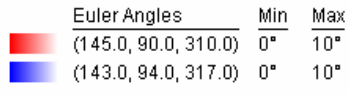

(b) crystal K2 and K1 at grain boundary, 12mm from the left top, as shown in Figure 3b

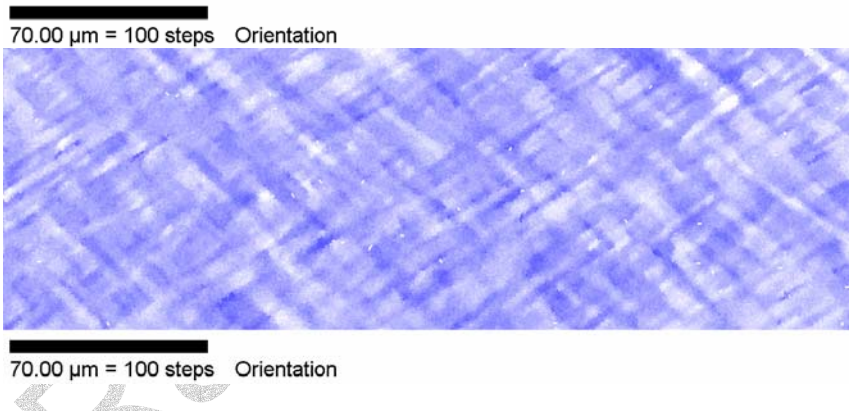

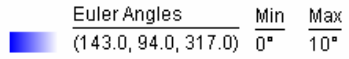

(c) crystal K1, 2mm away from the grain boundary

Figure 4: Microtexture mappings in regions close to the grain boundary with similar strain conditions in the 30% deformed bicrystal (EBSD step size: 700 nm, colour coding represents misorientation mapping selected separately in each area according to the local range in orientation change with respect to each initial orientation of crystal K1 and crystal K2).

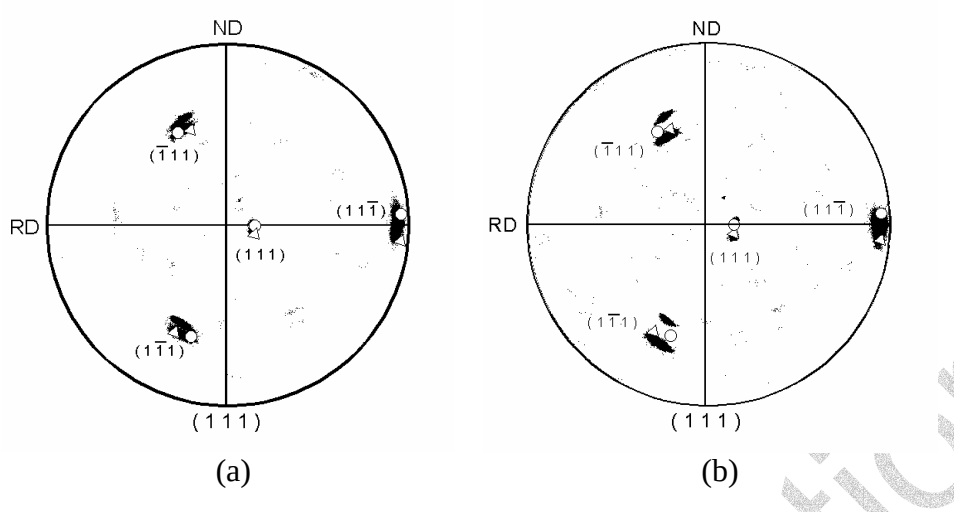

Figure 5: {111} pole figures measured by EBSD in the immediate vicinity of the grain boundary (a) and in the interiors of both crystals (b) in the 30% deformed bicrystal (O : initial orientation of crystal K1 and Δ : initial orientation of crystal K2). The data clearly show that the grain interiors reveal after straining a larger mutual misorientation than the areas close to the interface.